Synthesis, spectroscopic characterizations, cyclic voltammetry investigation and molecular structure of the high-spin manganese(III) trichloroacetato meso-tetraphenylporphyrin and meso-tetra-(para-bromophenyl)porphyrin complexes

W. Harhouri, S. Dhifaoui, Z. Denden, Thierry Roisnel, Fabian Blanchard, H. Nasri

Synthesis, spectroscopic characterizations, cyclic voltammetry investigation and molecular structure of the high-spin manganese(III) trichloroacetato *meso*-tetraphenylporphyrin and *meso*-tetra-(*para*-bromophenyl)porphyrin complexes

Wafa Harhouri*[a]*, *Selma Dhifaoui*[a], *Zouhour Denden*[a], *Thierry Roisnel*[b], *Florent Blanchard*[c] *and Habib Nasri*[a]

[a] *Laboratoire de Physico-chimie des Matériaux, University of Monastir, Faculté des Sciences de Monastir, Avenue de l'environnement, 5019 Monastir, Tunisia.*
[b] *Centre de Diffractométrie X, Institut des Sciences Chimiques de Rennes, UMR 6226, CNRS-Université de Rennes,1, Campus de Beaulieu, 35042 Rennes Cedex, France.*
[c] *ICSN Bât 27, 1 avenue de la Terrasse, 91190 Gif sur Yvette, France*

ABSTRACT

We present here the synthesis of two manganese(III) trichloroacetato porphyrins, namely (trichloroacetato)[5,10,15,20-tetraphenylporphyrinato]manganese(III) [Mn^{III}(TPP)(TCA)] (**1**) and (trichloroacetato)[(5,10,15,20-tetra-(*para*-bromophenyl)porphyrinato]manganese(III) hemi-chloroform hemi-dichloromethane solvates [Mn^{III}(TBrPP)(TCA)].1/2$CHCl_3$.1/2CH_2Cl_2 (**2**). These two new coordination compounds have been characterized by elemental analysis, UV-visible, IR and ^{1}H NMR spectroscopies, mass spectrometry, cyclic voltammetry and X-ray crystallography. The UV-visible spectra of **1** and **2** exhibit hyper type electronic spectra with very red shifted Soret bands, while the proton NMR spectra of these two Mn(III)-trichloroacetato metalloporphyrins present the β-pyrrole protons of the TPP and TBrPP porphyrinates as very upfield shifted bands, indicating that the two Mn(III) derivatives are high-spin (S = 2) with the ground state electronic configuration $(d_{xy}^1)(d_{xz,yz}^2)(d_{z^2}^1)$. The redox potential values of **1** and **2** are very close to each other and to other penta-coordinated high-spin Mn(III) metalloporphyrins. The average equatorial distance between the Mn cation and the nitrogen atoms of the porphyrin macrocycle (Mn–Np) of **1** and **2** are very close and are in the normal range for high-spin Mn(III) metalloporphyrins. The displacement of the manganese atom from the porphyrin mean plane (P_C) of the TBrPP derivative (**2**) is smaller than that of the TPP species (**1**) [0.147(1) and 0.236 (1) Å for **2** and **1** respectively], which is also the case for the deformations of the porphyrin core, where the TPP species (**1**) exhibits much higher *waving* and *saddle* deformations than the TBrPP derivative (**2**). Notably, the

* Corresponding author. Fax: +216 73 500 278.
E-mail address: hnasri1@gmail.com and habib.nasri@fsm.rnu.tn (Habib Nasri).

molecular structures of **1** and **2** present face to face π···π dimer formation with $P_C \cdots P_C$ distances of 3.69 and 3.88 Å, and Mn···Mn distances of 5.57 and 4.80 Å, respectively.

Keywords: Manganese(III) porphyrins, X-ray crystallography, UV-visible, Cyclic voltammetry

---

1. Introduction

Synthetic iron and manganese porphyrins resemble the active centers of heme-containing biological systems. Manganese porphyrins are also widely used in the biomimetic studies of cytochrome P-450 [1], catalases [2] and other enzymes [3]. Manganese porphyrins have proved to be efficient catalysts in the oxidation of olefins with single oxygen atom donors, such as iodosylbenzene [4], alkyl hydroperoxides [5], amine *N*- oxides [6] and hydrogen peroxide [7]. More recently in 2014, Simonneaux *et al*. reported the regioselective nitration of phenyl groups using a Mn(III) metalloporphyrin [8]. For manganese porphyrins, the central metal exhibits either the +II, +III or +IV oxidation states, with the most studied being the Mn(III) porphyrin derivative. Depending on the coordination and environment of the metal center, manganese porphyrins in the oxidation state +III are either five or six-coordinated. The majority of five-coordinated Mn(III)-porphyrin species are high-spin (S = 2), whereas all known six-coordinated Mn(III) porphyrins are low-spin (S = 1). The electronic properties of the high-spin Mn(III) porphyrin species are quite different from the other type of Mn(III) porphyrins and also from iron and cobalt metalloporphyrins, where the ground state electronic configuration of the Mn(III) center metal is $(d_{xy}^1)(d_{xz,yz}^2)(d_{z^2}^1)$ [9]. These high-spin Mn(III) derivatives with *meso*-porphyrins exhibit d-hyper type UV-visible spectra. Several investigations on five-coordinated high-spin Mn(III) porphyrins of the type [Mn^{III}(Porph)(X)], where X is a halide or pseudo-halide ligand, are reported in the literature [10]. Notably, the only reported acetato Mn(III) porphyrin species so far is the (acetate)(5,10,15,20-tetraphenylporphyrinato)manganese(III) coordination compound [9]. In order to get more insight on the spectroscopic, electrochemical and especially the structural properties of Mn(III) metalloporphyrins, trichloroacetato manganese(III) complexes with the 5,10,15,20-tetraphenylporphyrin (H_2TPP) and the 5,10,15,20-tetra-(*para*-bromophenyl)porphyrin (H_2TBrPP) were prepared and characterized. The effects of using two *meso*-porphyrins with different electron-donating/electron-withdrawing capabilities on the electronic and structural properties of the trichloroacetato Mn(III) metalloporphyrins will be discussed. Additionally, a

comparison of the two trichloroacetato Mn(III) species with the reported acetato *meso*-tetraphenylporphyrin manganese(III) is reported.

2. Experimental section

2.1. General information

All solvents and reagents were used as received. The 5,10,15,20-tetraphenylporphyrin (H_2TPP) and the 5,10,15,20-tetra-(*para*-bromophenyl)porphyrin (H_2TBrPP) were prepared according to the method of Adler *et al.* [11]. The metallation of the free-base porphyrins, leading to the Mn(III) acetato starting materials [Mn^{III}(Porph)(OAc)] (Porph = TPP, TBrPP), was performed as previously described [12]. The UV-visible spectra were recorded with a WinASPECT PLUS (validation for SPECORD PLUS version 4.2) scanning spectrophotometer. The FTIR spectra were recorded with a Perkin Elmer Spectrum Two FTIR spectrometer. The ^{1}H NMR spectra were obtained at room temperature with a Bruker 300 Ultra shield spectrometer. Cyclic voltammetry (CV) experiments were performed with a CH-660B potentiostat (CH Instruments). All analytical experiments were conducted at room temperature under an argon atmosphere in a standard one-compartment, three-electrode electrochemical cell. Tetra-n-butylammonium hexafluorophosphate ($TBAPF_6$) was used as the supporting electrolyte (0.2 M) in dichloromethane previously distilled over calcium hydride under argon. An automatic Ohmic drop compensation procedure was systematically implemented before the CV data were recorded with electrolytic solutions containing the studied compounds at concentrations of ca. 10^{-3} M. CH Instruments vitreous carbon (Ø = 2 mm) working electrodes were polished with 1 µm diamond paste before each recording. The saturated calomel electrode SCE ($TBAPF_6$ 0.2 M in CH_2Cl_2) redox couple was used as the reference electrode. The potential of the ferrocene / ferrocenium redox couple was used as an internal reference (0.37 V/SCE experimental conditions).

*2.2. Preparation of complexes **1** and **2***

2.2.1. Synthesis of (trichloroacetato)[5,10,15,20-tetraphenylporphyrinato]manganese(III) [Mn^{III}(TPP)(TCA)] (**1**)

Sodium trichloroacetate (80 mg, 0.431 mmol) and cryptand-222 (60 mg, 0.159 mmol) were stirred together in chlorobenzene (10 mL). [Mn^{III}(TPP)(OAc)] (100 mg, 0.137 mmol) in chlorobenzene (10 mL) was added to the trichloroacetate/cryptand solution and the mixture was stirred for 4 h. The solution was filtered and crystals of the [Mn^{III}(TPP)(TCA)] (**1**) complex were prepared by slow diffusion of n-hexane into the chlorobenzene solution (97

mg, yield ~ 85 %).

Anal. Calc. for (**1**), $C_{46}H_{28}Cl_3MnN_4O_2$ (830.03 g/mol): C, 66.56; H, 3.4; N, 6.75%. Found: C, 66.61; H, 3.55; N, 6.68%. UV-visible [λ_{max} (nm) in CH_2Cl_2, (logε)]:383 (5.70), 404 (5.68), 475 (6.02), 575 (5.23), 609 (5.17) ^{1}H NMR (300 MHz, $CDCl_3$, 298 K) δ (ppm): -26.35 (s, 8 H, pyrrole β-H), 8.23 (s, 16 H, TPP *o*-H, m-H). FTIR (KBr disk, cm^{-1}) $\bar{\nu}$: 1692 (C=O carbonyl, TCA ligand), 1302 (C-H, TCA ligand).

2.2.2. Synthesis of tricloroacetato[(5,10,15,20-tetra-(para-bromophenyl)porphyrinato]manganese(III) hemi-chloroform hemi-dichloromethane solvates $[Mn^{III}(TBrPP)(TCA)].1/2CHCl_3.1/2CH_2Cl_2$ (**2**)

Complex **2** was prepared by the procedure given for **1**, except that the TBrPP porphyrinato ligand was used instead of TPP. Good quality crystals of **2** were obtained by slow diffusion of n-hexane through the chloroform/dichloromethane (1/1) solution of this species (127 g, yield ~ 80 %).

Anal. Calc. for (**2**), $C_{47}H_{25.5}Br_4Cl_{5.5}MnN_4O_2$ (1247.79 g/mol): C, 45.24; H, 2.06; N, 4.49%. Found: C, 45.61; H, 2.15; N, 4.62%. UV-visible [λ_{max} (nm) in CH_2Cl_2, (logε)]: 380 (5.84), 403(5.82), 474 (6.05), 575 (5.37), 610 (5.30). ^{1}H NMR (300 MHz, $CDCl_3$, 298 K): δ(ppm) : -26.63 (s, 8 H, pyrrole β-H), 8.35 (s, 16 H, TBrPP*o*-H, *m*-H).). FTIR (KBr disk cm^{-1}): $\bar{\nu}$ = 1689 (C=O carbonyl, TCA ligand), $\bar{\nu}$ = 1298 (C-H, TCA ligand).

2.3. X-ray structure determination

The data collection for **1** was performed with a D8 VENTURE, Bruker, diffractometer (at 150 K) while the data collection of **2** was measured using a Rigaku Pilatus diffractometer (at 293 K). Both devices were equipped with a graphite-monochromated Mo-Kα radiation source (λ = 0.71073 Å). The reflections concerning complex **1** were scaled and corrected for absorption effects using the SADABS program version 2.10 (Bruker AXS 2001) [13]. For **2**, the CrysAlisPro program [14] was used for the data absorption correction. The structures of **1** and **2** were solved by direct methods using SIR-2004 [15] and olex2.solve [16] programs (using the Charge Flipping solution method), respectively. Both structures were refined by full-matrix least-squares techniques on F^2 by using the SHELXL-97 program [17].

For **1**, the chlorine atoms of the trichloroacetato (TCA) ligand were disordered over two positions (CL1A-CL2A-CL3A and CLIB-CL2B-CL3B) with occupancy factors 0.833(2) and

0.167(2), respectively. Complex **2** presents a half chloroform and a half dichloromethane in the asymmetric unit, which have very high ADP values indicating a static disorder. For these solvent molecules, the DFIX, DANG and SIMU constraint commands in the SHELXL-97 software were used [18]. The crystallographic data, the structural refinement details and selected bond lengths and angles for **1** and **2** are reported in Table 1. Selected bond distances and angles for **1** and **2** are listed in Table 2.

Table 1. Crystal data and structural refinement for $[Mn^{III}(TPP)(TCA)]$ (**1**) and $Mn^{III}(TBrPP)(TCA)].1/2CHCl_3.1/2CH_2Cl_2$ (**2**)

Compound	**1**	**2**
Formula	$C_{46}H_{28}Cl_3MnN_4O_2$	$C_{47}H_{25.5}Br_4Cl_{5.5}MnN_4O_2$
D_{calc} (g cm^{-3})	1.509	1.839
M (mm^{-1})	0.63	4.212
Formula Weight	830.01	1247.77
Color	Black	Brown
Size (mm^3)	0.57 × 0.48 × 0.40	0.15 × 0.07 × 0.06
T (K)	150(2)	293(2)
Crystal System	Monoclinic	Triclinic
Space Group	*P2₁/n*	*P-1*
a (Å)	11.4101(8)	10.0347(8)
b (Å)	22.6604(13)	16.0008(9)
c (Å)	14.6652(10)	16.5729(11)
α (°)	90	110.699(5)
β (°)	105.477(2)	106.929(6)
γ (°)	90	100.761(6)
V($Å^3$)	3654.3(4)	2253.2(3)
Z	4	2
F(000)	1696	1220
θ_{min} (°)-θ_{max} (°)	3.019 – 26.000	3.678 – 26.000
Limiting indices	-14≤ h ≤14, -27≤ k ≤27, -18≤ l ≤18	-12≤ h ≤12, -19≤ k ≤19, -20≤ l ≤20
T_{min}, T_{max}	0.710, 0.778	0.440, 1.000
Total reflections	24638	37012
Independent reflections	7145	8830
Reflections used	5530	5908
R_{int}	0.035	0.079
Parameters	515	604
GooF (*S*)	1.021	1.038
wR_2 (all data)	0.1533	0.159
wR_2 [a]	0.1397	0.139
R_1 (all data)	0.0841	0.094
R_1 [b]	0.0622	0.057
Δ_ρ (max, min) (e/$Å^3$)	1.17, -1.00	0.91, -0.83
CCDC	1515031	1510380

[a] : $wR2 = \{\Sigma[w(|F_O|^2 - |F_C|^2)^2]/\Sigma[w(|F_O|^2)^2]\}^{1/2}$, [b] : $R_1 = \Sigma||F_O| - |F_C||/\Sigma|F_O|$.

Table 2. Selected bond lengths [Å] and angles [°] for **1** and **2**.

Complex **1**		Complex **2**	
	Manganese coordination polyhedron		
Mn–N1	2.002(3)	Mn–N1	2.010(4)
Mn–N2	2.011(3)	Mn–N2	2.007(4)
Mn–N3	1.996(3)	Mn–N3	2.003(4)
Mn-N4	2.015(3)	Mn-N4	2.012(4)
Mn-Np	2.006(3)	Mn-Np	2.008(4)
Mn-O1	2.054(3)	Mn-O1	2.057(4)
N1–Mn–N2	89.55(11)	N1–Mn–N2	89.41(16)
N3–Mn–N4	89.28(12)	N3–Mn–N4	89.62(16)
N1–Mn–N3	170.99(12)	N1–Mn–N3	170.15(18)
N1–Mn–N4	89.15(11)	N1–Mn–N4	89.34(16)
N2–Mn–N3	89.28(11)	N2–Mn–N3	89.30(16)
N2–Mn–N4	162.48(12)	N2–Mn–N4	166.40(18)
	Trichloroacetato(TCA) axial ligand		
O1–C45	1.254(5)	O1–C45	1.221(7)
O2-C45	1.178(5)	O2-C45	1.198(8)
C45-C46	1.586(5)	C45-C46	1.574(9)
C46-Cl1A	1.751(4)	C46-Cl1	1.737(8)
C46-Cl1B	1.871(11)	C46-Cl2	1.750(7)
C46-Cl2A	1.767(5)	C46-Cl3	1.756(7)
C46-Cl2B	1.555(10)		
C46-Cl3A	1.790(5)		
C46-Cl3B	1.630(13)		

3. Results and discussion

3.1. UV-visible and NMR ^{1}H spectroscopy

3.1.1. UV-visible spectroscopy

The UV-visible spectra of **1** and **2** are illustrated in Figure 1. It is noteworthy that the manganese(III) *meso*-porphyrins present hyper type electronic spectra with a half unoccupied metal orbital with symmetry e_g [d_π :d_{xz} and d_{yz}] (Figure SI-1) [9]. The intense band in the range 440-480 nm is known as the charge transfer band or the Soret band (band V). This band is attributed to the transfer from the $a_{1u}(\pi)$ and $a_{2u}(\pi)$ orbitals of the porphyrin to the manganese e_g [$d\pi$: d_{xz} and d_{yz}] orbitals. In the UV region, two other bands, namely (VI) and (Va) (less intense than the Soret band), are observed between 350 and 410 nm. In the visible region, two absorption bands (QIII and QIV) are shown in the range 560 to 620 nm, while the

bands QI and QII are shifted in the infrared region and cannot be found in the electronic spectra [19]. For complexes **1** and **2**, the λ_{max} values of the (VI), (Va), Soret (V), (QIV) and (QIII) bands are practically the same: ~ 380, ~ 403, ~ 475, ~ 575 and ~ 610 nm, respectively (Table 3). The UV-vis data of the Mn(III)-metalloporphyrins are also very close. Therefore, the nature of the axial ligands and the *meso*-porphyrins have little effect in the electronic spectra of the manganese(III) porphyrin derivatives. This could be explained by the charge transfer between the $a_{1u}(\pi)$ and $a_{2u}(\pi)$ orbitals of the porphyrin to the $e_g[d\pi]$ orbitals of Mn(III) center metal which "dominates" the electronic transitions of these species.

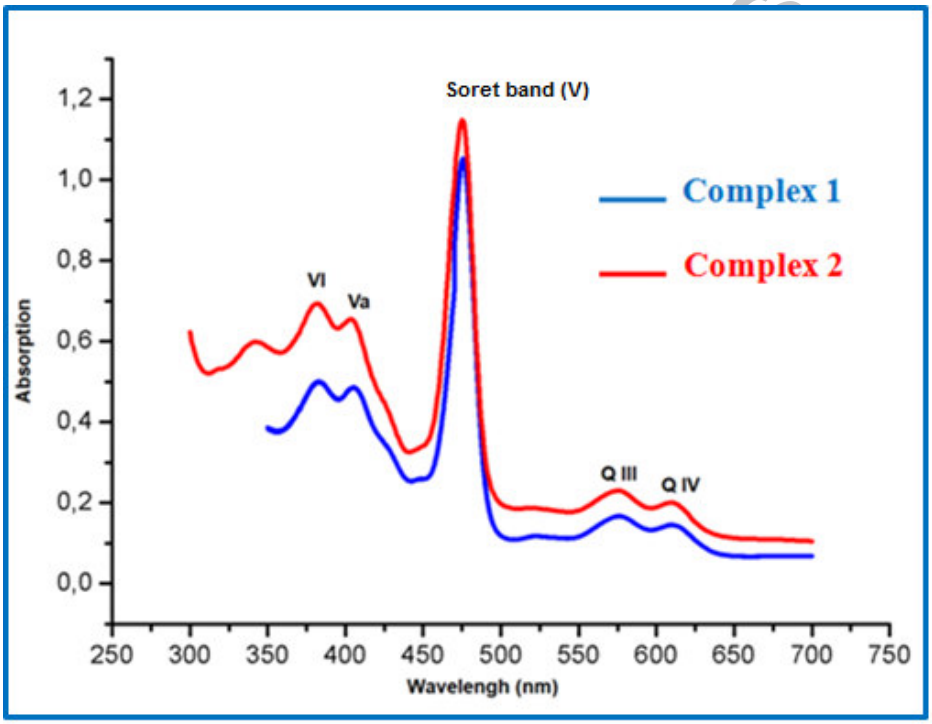

Figure 1. UV/Vis absorption spectra of $[Mn^{III}(TPP)(TCA)]$ (**1**) and $[Mn^{III}(TBrPP)(TCA)].1/2CHCl_3.1/2CH_2Cl_2$ (**2**), in dichloromethane solution at concentrations of ca. 10^{-6} M.

Table 3. UV-visible data of **1** and **2** and selected manganese(III) metalloporphyrins. The spectra are recorded in dichloromethane (exceptions are indicated).

Complex	(QVI) band	(Va) band	Soret band	(QIII)and(QIV) bands	Ref.

	λ_{max} [nm] (log ε)					
[Mn(TMPP)Cl][a]	371	397	**475**	587	624	**[19]**
$[Mn(TPP)(SO_4)]^-$	374(4.91)	397(4.86)	**466**(5.23)	575(4.18)	612(4.13)	**[20]**
$[Mn(TPP)(HSO_4)]$	384(4.75)	405	**470**(4.71)	574(3.85)	608(3.77)	**[20]**
$[Mn(TPP)(NO_3)]$[b]	384(4.64)	406(4.61)	**478**(4.9)	577(3.93)	611(3.86)	**[21]**
$[Mn(TPP)(NO_2)]$[b]	380(4.71)	400(4.69)	**476**(4.94)	583(3.89)	620(3.95)	**[21]**
$[Mn(TPP)(ClO_4)(py)]$[c]	-	417	**477**	585	614	**[22]**
$[Mn(TPP)(H_2O)]SO_3CF_3$	386	-	**474**	570	604	**[23]**
[Mn(TPP)(TCA)] (**1**)	383(5.70)	404(5.68)	**475**(6.02)	575(5.23)	609(5.17)	this work
[Mn(TBrPP)(TCA)] (**2**)	380(5.84)	403(5.82)	**474**(6.05)	575(5.37)	610(5.30)	this work

[a]: TMPP = 5,10,15,20-tetra(4-methyl-phenyl)porphyrinato, [b]: Solvent = benzene, [c]: Solvent = chloroform.

3.1.2. Proton NMR spectroscopy

The chemical shifts (δ) of the β-pyrrole protons of complexes **1** and **2**, as well as several Mn(III) high-spin *meso*-porphyrins, are given in Table 4 where we can see that five-coordinated high-spin (S = 2) Mn(III) *meso*-porphyrins exhibit downfield chemical shift values. Our Mn(III) compounds **1** and **2** present very close δ values (-26.4 and -26.8 ppm respectively), indicating a high-spin character in solution. P. Turner *et al.*, [24] correlated the chemical shift values of the β-pyrrole protons of several high-spin Mn(III) penta-coordinated *meso*-porphyrins of the type $[Mn^{III}(Porph)(X)]$ (where X is an anionic axial ligand) to the π-donor character of the axial ligand. Thus, the δ values shift to the upfield region with decreasing π-basic character, e.g. for the $[Mn^{III}(TPP)F]$, $[Mn^{III}(TPP)(OAc)]$ and $[Mn^{III}(TPP)I]$ complexes, the δ values are -19.7, -21.8 and -25.9 ppm, respectively [24]. The chemical shift values of the β-pyrrole protons of **1** and **2** are smaller than that of the Mn(III)-acetato derivative (δ = -21.8 ppm). This could be explained by the weaker π-donor character of the trichloroacetato ligand compared to the acetato ligand. This result was also confirmed by the molecular structures of **1** and **2** (see crystallographic section).

Table 4. Chemical shift values of the β-pyrrole protons of **1-2** and selected five-coordinated manganese(III) porphyrins.

Complex	β-pyrrole (ppm)	Ref.

[Mn^{III}(TPP)F]	-19.7	[24]
[Mn^{III}(TPP)(OAc)]	-21.8	[24]
[Mn^{III}(TPP)(N_3)]	-22.1	[24]
[Mn^{III}(TPP)Cl]	-22.3	[24]
[Mn^{III}(TPP)Br]	-23.5	[24]
[Mn^{III}(TPP)I]	-25.9	[24]
[Mn^{III}(TPP)(NO_2)]	-27.3	[24]
[Mn^{III}(TPP)(NO_3)]	-28.0	[24]
[Mn^{III}(TPP)(ClO_4)]	-36.0	[24]
[Mn^{III}(TPP)(TCA)] (**1**)	-26.4	this work
[Mn^{III}(TBrPP)(TCA)] (**2**)	-26.6	this work

3.3. Cyclic voltammetry

Previous studies on the cyclic voltammetry of five-coordinated manganese(III) porphyrins of the type [Mn^{III}(Porph)(X)] (Porph = *meso*-porphyrinato and X = halogeno or pseudo-halogeno ligand) have shown that: (i) these species exhibit a one electron reversible wave corresponding to the Mn(III)/Mn(II) reduction, (ii) potentials values for the second (and third) reduction waves are attributed to reductions of the porphyrin macrocycle and (iii) two one electron oxidation waves are attributed to the oxidation of the porphyrin core [25-27]. The $E_{1/2}$ potential values of the oxidations and reductions of the [Mn^{III}(Porph)(X)] derivatives depend on the nature of the porphyrin, the type of X axial ligand and the solvent used [25-27]. Figure 2 represents the cyclic voltammograms (CV) of our TCA-Mn(III) derivatives (**1** and **2**), while in Table 5 the CV data of **1** and **2** and other related Mn(III) metalloporphyrins are summarized. For **1** and **2**, the first one electron reversible waves corresponding to the Mn(III)/Mn(II) reduction (R3/O3) present half potential values at -0.33 and -0.38 V, respectively, which are close to other related Mn(III) species (Table 5). For the Mn-TPP derivative (**1**), the first reduction wave is irreversible, with an anodic potential (O3) of -1.48 V, and the second reduction wave is quasi-reversible with an $E_{1/2}$ value of -1.70 V. For the Mn-TBrPP species (**2**), the half potential value of the first quasi-reversible wave (R4/O4) is -1.49 V and the value of the cathodic irreversible wave is -1.70 V.

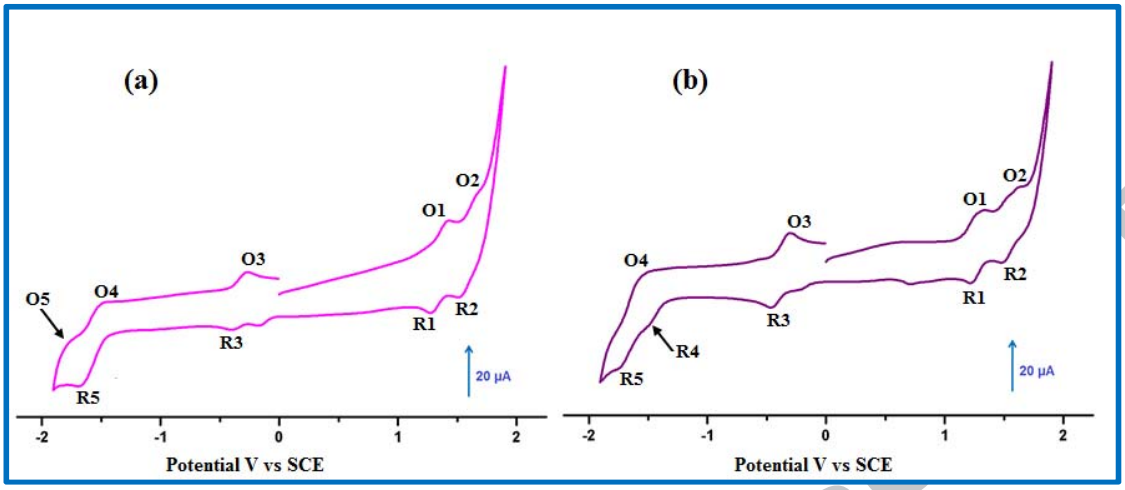

Figure 2. Cyclic voltammograms of **1** (a) and **2** (b). The solvent is CH_2Cl_2 and the concentration is ca. 10^{-3} M in 0.2 M $TBAPF_6$, 100 mV/s, vitreous carbon working electrode (Ø = 2 mm).

These waves are attributed to the first and second reductions of the porphyrin core of **1** and **2**, which are in the range of other manganese(III) metalloporphyrins. The voltammograms of our two synthetic Mn species present one reversible oxidation wave (O1/R1) and one quasi-reversible oxidation wave (O2/R2) attributed to the oxidations of the porphyrin ring. Indeed, the half potential values of the first oxidation waves are 1.34 and 1.25 V for **1** and **2**, respectively, while the $E_{1/2}$ values for the second oxidation waves are 1.58 and 1.56 V for **1** and **2**, respectively. We noticed that the redox potentials values of **1** and **2** are very close, indicating that the nature of the group in *para* position to the phenyl group of the *meso*-porphyrin have practically no effect on the electrochemical properties of our two trichloroacetato-Mn(III) derivatives. These potential values of **1** and **2** are close to other manganese(III) porphyrins. The voltammograms of **1** and **2** also exhibit weak waves, other than those mentioned above, which could be attributed to the electrochemical reactions of other species related to the TCA ligand.

Table 5. Electrochemical data[a] for complexes **1** and **2** and a selection of Mn(III) metalloporphyrins.

Complex	Oxidations									Reductions						Ref.
	Ring oxidations						Metal reduction Mn(III)/Mn(II) (R3,O3)			Ring reductions						
	1st oxidation (O1,R1)			2nd oxidation (O2,R2)						1st reduction (R4,O4)			2nd reduction (R5,O5)			
	E_{pa}[b]	E_{pc}[c]	$E_{1/2}$[d]	E_{pa}[b]	E_{pc}[c]	$E_{1/2}$[d]	E_{pc}[b]	E_{pa}[c]	$E_{1/2}$[d]	E_{pc}[b]	E_{pa}[c]	$E_{1/2}$[d]	E_{pc}[b]	E_{pa}[c]	$E_{1/2}$[d]	
[Mn(TPP)Cl]	-	-	1.14[e]	-	-	-	-	-	-0.29[e]	-	-	-1.52[e]	-	-	-	[26]
												-1.28[f]	-	-	-1.77	
[Mn(TPP)(N_3)]	-	-	1.18[e]	-	-	-	-	-	-0.34[e]	-	-	-1.52[e]	-	-	-	[26]
[Mn(TPP)(SCN)]	-	-	1.19[e]	-	-	-	-	-	-0.25[e]	-	-	-1.57[e]	-	-	-	[26]
[Mn(TPP)Cl]	-	-	1.28[g]	-	-	1.64[g]	-	-	-0.21[g]	-	-	-1.47[g]	-	-	-1.79[g,*]	[27]
[Mn(TPP)(TCA)] (**1**)	1.41	1.28	1.34	1.64	1.52	1.58	- 0.40	-0.27	-0.33	-	-1.48	-	-1.65	-1.76	-1.70	this work
[Mn(TBrPP)(TCA)] (**2**)	1.29	1.21	1.25	1.62	1.50	1.56	-0.46	-0.30	-0.38	-1.46	-1.52	-1.49	-1.70	-	-	this work

[a]:The potentials (values in Volt) are reported versus SCE, [b]: E_{pa} = anodic peak potential. [c]: E_{pc} = cathodic peak potential, [d]: $E_{1/2}$ = half wave potential, [e]: in dichloromethane solvent. [f]: in DMSO solvent. [g]: in benzonitrile solvent, *: denotes an irreversible wave.

3.4. X-ray molecular structures

The Mn(III)-trichloroacetato (TCA) complex with the TPP porphyrinate (**1**) crystallizes in the monoclinic system ($P2_1/n$ space group), where the crystals were obtained by slow diffusion of n-hexane through a chlorobenzene solution of the complex. Crystals of the Mn(III)-TCA derivative with TBrPP (**2**) were obtained by slow diffusion of n-hexane through a chloroform / dichloromethane (1/1) mixture. This species crystallizes in the triclinic crystal system (*P-1* space group). The molecular structures of **1** and **2** are illustrated in Figure 3.

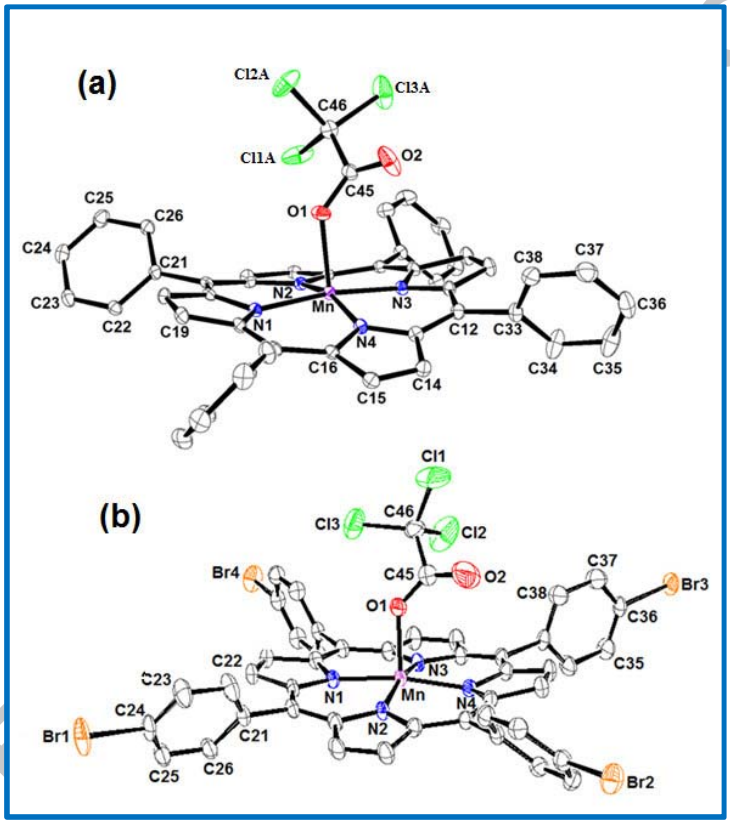

Figure 3. (a): ORTEP diagram of [Mn^{III}(TPP)(TCA)] complex (**1**), (b): ORTEP diagram of [Mn^{III}(TBrPP)(TCA)] complex (**2**). Ellipsoids are contoured at the 50% probability level for both **1** and **2**. For the TPP derivative (**1**), only the major position of the CCl_3 moiety of the TCA ligand is represented. The chloroform and dichloromethane solvents of complex **2** are omitted for clarity.

The asymmetric unit of **1** is made from one [Mn^{III}(TPP)(TCA)] complex, while the asymmetric unit of **2** contains one [Mn^{III}(TBrPP)(TCA)] complex, a half chloroform and a half dichloromethane solvent molecule. The Mn^{III} cation is chelated by the four pyrrole N atoms of the porphyrinate anion and additionally coordinated by the trichloroacetato (TCA)

ligand in an apical site, completing the distorted square-pyramidal coordination environment (Figure 4). The Mn—O(TCA) distance values of **1** and **2** are very close [2.053(3) and 2.057(4) Å, respectively] which are quite a bit longer than those of the acetato related species [Mn^{III}(TPP)(OAc)] (Table 6) [9] with values of 2.028(5) and 2.010(5) Å (the asymmetric unit of this species contains two [Mn^{III}(TPP)(OAc)] molecules). This is also the case for the related iron(III) species with acetato (OAc), trifluoroactato (TFA) and trichloroactetato (TCA) (Table 7) where the Fe—O_L (L = OAc, TFA and TCA) distance increases from the OAc to the TFA and TCA derivatives (Table 6). The fact that the M—O_L [M = Fe(III) or Mn(III)] distances in **1** and **2** and the related halogeno-acetato iron(III) metalloporphyrins are longer than those of the M—O(OAc) derivatives could be explained by the attractor character of the CF_3 and CCl_3 moieties compared to the CH_3 group. The C45-O1-Mn angle values of **1** and **2** are very close [137.6(3) and 135.3(5)°, respectively], and they are larger than those of the [Mn^{III}(TPP)(OAc)] related derivative [128.6(5) and 131.5(6)°], reflecting the closer approach of the TCA ligand to the porphyrin macrocycle. The same trend is observed for the acetato-iron(III) porphyrin species where the C-O-Fe angle values decrease from the trichloroacetato (TCA) to the trifluoroacetato (TFA) and finally to the acetato (OAc) species (Table 7). All bond lengths for the TCA ligand in **1** and **2** are very close (Table 2). Formal diagrams showing the displacements of the atoms (in units of 0.01 Å) from the 24-atom mean plane of complexes **1** and **2** are illustrated in Figure 5, while in Figure SI-2, the formal diagram of the porphyrin core of the related complex [Mn^{III}(TPP)(OAc)] is shown [9]. The porphyrin core presents four major deformations [28,29]. The *doming* distortion (*dom*) is observed when the nitrogen atoms of the pyrrole rings are displaced above the porphyrin cycle. In the *waving* distortion (*wav*), the four fragments «(β-carbon)-(α-carbon)-(*meso*-carbon)-(α-carbon)-(β-carbon)» (or Cβ-Cα-Cm-Cα'-Cβ') are alternatively above and below the 24-atoms of the $C_{20}N_4$ least squares plane of the porphyrin core. For the *saddle* deformation (*sad*), the pyrrole rings are alternatively displaced above and below the porphyrin core. The *ruffling* deformation (*ref*) of the porphyrin core is shown when the *meso* carbons are alternatively above and below the porphyrin mean plan. The Mn-TCA-TPP derivative (**1**), exhibits very high *wav* and *sad* deformations and moderate *ref* and *dom* distortions of the porphyrin core (Figures 5 and 6). For the Mn-TCA-TBrPP derivative (**2**), the porphyrin macrocycle presents high *wav* and *sad* distortions but less than complex **1**. This complex presents also a weak *dom* and very weak *ref* distortion of the porphyrin macrocycle (Figures 5 and 6).

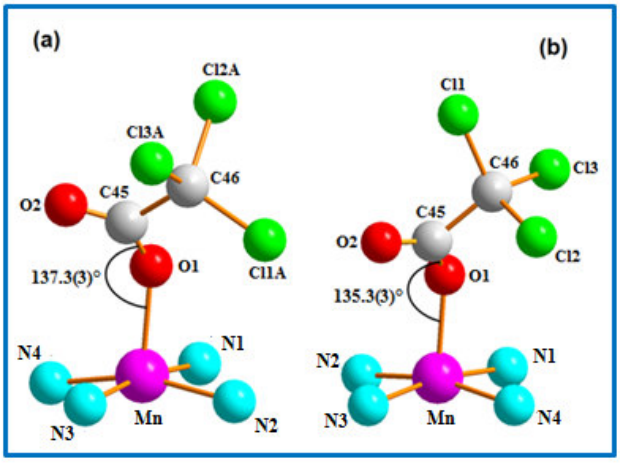

Figure 4. Coordination polyhedra of the Mn center metal in [Mn^{III}(TPP)(TCA)] (**1**): (a) and [Mn(TBrPP)(TCA)] (**2**): (b).

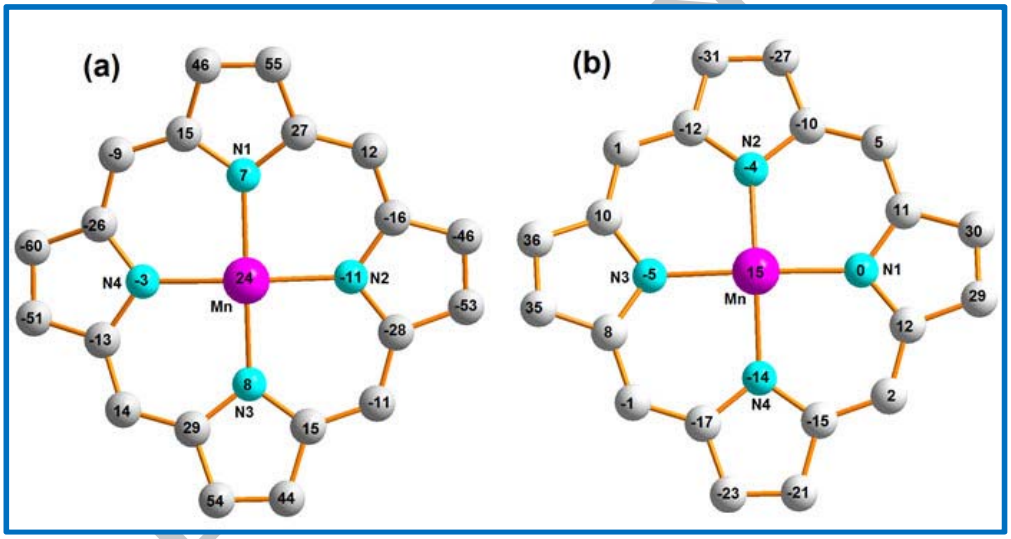

Figure 5. Formal diagrams of the porphyrinato cores of **1**: (a) and **2**: (b). The displacement of each atom from the mean plane of the 24-atom porphyrin macrocycle in given in units of 0.01 Å.

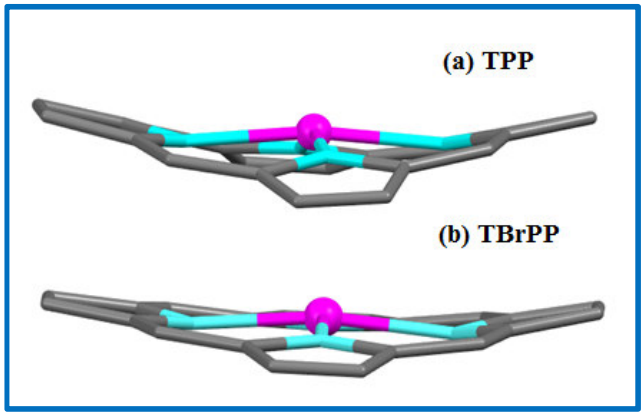

Figure 6. Schematic representations showing the porphyrin core deformations of **1** and **2**.

It is noticeable that for the Mn-OAc-TPP related species, one of the two [Mn^{III}(TPP)(OAc)] molecules present high *wav* and *sad* deformations comparable to our Mn-TCA-TPP species (**1**). The fact that both Mn(III)-OAc and Mn(III)-TCA TPP derivatives exhibit similar higher deformations than those of the Mn-TCA-TBrPP species is presumably due to the nature of the porphyrin and not the OAc and TCA ligands. The electron density of the porphyrin core of TBrPP porphyrinato is higher than TPP porphyrinato because of the strong electron donation character of the bromine atoms in the *para* positions of the phenyl groups of the TBrPP ligand. This leads to the enhancement of the aromaticity of the porphyrin core of the TBrPP moiety and therefore diminishes the deformations of the macrocycle.

Several investigations on the ground-state electronic configurations of Mn(II) and Mn(III) metalloporphyrins are reported in the literature [30,31] which correlate the oxidation state and the spin state of the manganese center metal with the average equatorial distance between the Mn cation and the nitrogen atoms of the porphyrin macrocycle (Mn—Np). According to these studies, five-coordinated Mn(II) porphyrin complexes of the type [Mn^{II}(Porph)(L)] (Porph = porphyrin and L is a monodentate neutral ligand) are high-spin (S = 5/2) with the ground-state electronic configuration $(d_{xy}^1)(d_{xz,yz}^2)(d_{z^2}^1)(d_{x^2-y^2}^1)$. Five-coordinated Mn(III) metalloporphyrins with halogeno or pseudo-halogeno axial ligands of the type [Mn^{III}(Porph)(X)] (X = halogeno or pseudo-halogeno ligand) are high-spin (S = 2) with the electronic configuration $(d_{xy}^1)(d_{xz,yz}^2)(d_{z^2}^1)$ [9]. The stereochemistry of the Mn(II) and Mn(III) five-coordinated high-spin complexes is expected to be dominated by the size of the metal atom. Since the $d_{x^2-y^2}$ orbital is occupied in high-spin (S = 5/2) Mn(II) species, the size of the metal ion will be of importance. Consequently, the manganese(II) porphyrins

exhibit a high Mn—Np distance value and also a high displacement of the Mn(II) central metal from the porphyrin core (Mn--P_C). For five-coordinated Mn(III) high-spin derivatives (S = 2), the $d_{x^2-y^2}$ orbital in not occupied, leading to much lower Mn—Np and Mn—P_C distance values than those of five-coordinated high-spin (S = 5/2) Mn(II) porphyrins. For our Mn(III)-TCA derivatives (**1** and **2**), the Mn—Np values are 2.005(3) and 2.008(4) Å for **1** and **2**, respectively, while the Mn--P_C values are 0.236(1) and 0.147(1) Å, respectively. The M—Np and Mn—P_C distance values of the acetato related species [Mn^{III}(TPP)(OAc)] are 2.019(7)/2.021(6) and 0.286(1)/0.276(1) Å, respectively. Therefore, we can deduce from these distances for **1** and **2** in the solid state that the TCA-Mn(III) derivatives are high-spin (S = 2) Mn(III) metalloporphyrins.

Table 6**.** Selected bond lengths [Å] and angles [°] for **1** and **2** and several five-coordinated manganese(II) and manganese(III) metalloporphyrins.

Complex	Mn—N_P[a] (Å)	Mn—N_L[b]	(Å)	Mn—P_C[c] (Å)	Ref.
	Manganese(II) porphyrins				
[Mn^{II}(TpivPP)(1-MeIm)]	2.1285(6)	2.168(5)	0.56		[32]
[Mn^{II}(TpivPP)(1-EtIm)]	2.122(3)	2.216(19)	0.54		[32]
Mn^{II}(TpivPP)(2-MeHIm)]	2.129(3)	2.177(9)	0.60		[32]
[Mn^{II}(TPP)(1-MeIm)]	2.128(7)	2.192(2)	0.56		[33]
	Manganese(III) porphyrins				
[Mn^{III}(TPP)Cl]	2.008(5)	2.381(3)	0.262		[9]
[Mn^{III}(TPP)Br]	2.013(3)	2.490(1)	0.317(1)		[9]
[Mn^{III}(TPP)I]	2.015(5)	2.767(1)	0.207(1)		[9]
	2.017(6)	2.730(1)	0.236(1)		
[Mn^{III}(TPP)(NCO)]	2.013(5)	2.029(5)	0.339(1)		[9]
[Mn^{III}(TPP)(NCS)]	2.002(6)	2.067(6)	0.236(1)		[9]
	2.004(7)	2.072(5)	0.231(1)		
[Mn^{III}(TPP)(NO_3)]	2.007(4)	2.101(4)	0.191		[21]
[Mn^{III}(TPP)(NO_2)]	2.012(4)	2.059(4)	0.194		[21]
[Mn^{III}(TPP)(HSO_4)]	1.991(8)	2.077(9)	0.227		[20]
[Mn^{III}(TPP)(OAc)][d]	2.019(7)	2.028(5)	0.286(1)		[9]
	2.021(6)	2.010(5)	0.276(1)		
[Mn^{III}(TPP)(TCA)] (**1**)	2.005(3)	2.053(3)	0.236(1)		this work
[Mn^{III}(TBrPP)(TCA)] (**2**)	2.008(4)	2.057(4)	0.147(1)		this work

[a]: Mn—N_P = average equatorial Mn–$N_{pyrrole}$ bond length, [b]: Mn—N_L = distance between the metal and the axial ligand, [c]: Mn—P_C = distance between the metal atom and the mean plane made by the 24-atom core of the porphyrin (P_C), [d]: OAc = acetato ligand.

Table 7. Selected bond lengths [Å] and angles [°] for **1** and **2**, and some acetato and trichloroacetato iron(III) and Mn(III) metalloporphyrins.

Complex	M—N_P[a] (Å)	M—O_L[b] (Å)	M—P_C[c] (Å)	M—O—C (°)	M···M (Å)	P_C···P_C (Å)	Ref.
			Iron(III) complexes				
[Fe^{III}(OEP)(TCA)][d,e]	2.045(6)	1.928(2)	0.450	131.65(2)	5.38	4.71	[34]
[Fe^{III}(TPP)(TFA)][f]	2.054(5)	1.921(4)	0.483(1)	129.3(6)	9.754	4.21	[35]
[Fe^{III}(TPP)(OAc)][g]	2.070(2)	1.913(1)	0.523	121.03(1)	8.625	4.52	[36]
			Manganese(III) complexes				
[Mn^{III}(TPP)(OAc)]	2.019(7)	2.028(5)	0.286(1)	128.6(5)	5.875	3.787	[9]
	2.021(6)	2.010(5)	0.276(1)	131.5(6)°			
[Mn^{III}(TPP)(TCA)] (**1**)	2.005(3)	2.053(3)	0.236(1)	137.6(3)°	5.570	3.697	this work
[Mn^{III}(TBrPP)(TCA)] (**2**)	2.008(4)	2.057(4)	0.147(1)	135.3(5)°	4.801	3.888	this work

[a]: M—Np = average equatorial metal–Npyrrole bond length, [b]: M—O_L = metal-oxygen atom (of the axial ligand) distance, [c]: M—P_C = metal-24 atom porphyrin core (P_C) distance, [d]: OEP = octaethylporphyrinato. [e]: TCA = trichloroacetato, [f]: TFA = trifloroacetato, [g]: OAc = actetato.

The most important feature of the crystal structures of **1** and **2** is the face to face π—π dimer formation. Such a type of porphyrin dimers is characterized by several parameters which are the $P_C \cdots P_C$ and Mn···Mn distances, and the lateral shift (L.S.) which represents the "slipped" arrangement of the two porphyrins macrocycles (Figure 7). The L.S. is define by the relationship L.S. = [sin(S.A.).($P_C \cdots P_C$)] where S.A. is the "slip angle" between the two porphyrins cores [37]. Thus, when the two porphyrin rings are related by an inversion center, which is the case for **1** and **2**, these two porphyrin cores will be precisely parallel and the vector joining opposite nitrogen atoms in one macrocycle is parallel to that in the second porphyrin ring (see Figure-SI-3).

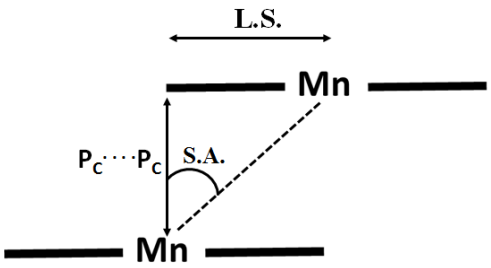

Figure 7. Schematic illustration of $P_C \cdots P_C$, Mn···Mn, the lateral shift (L.S.) and the shift angle (S.A.) of a Mn(III) porphyrin dimer.

Figure 8 is a schematic representation of the dimers of complexes **1** and **2**, while Figure SI-4 illustrates the dimer of [Mn^{III}(TPP)(OAc)] [9]. The $P_C \cdots P_C$ distances of **1** and **2** and the OAc-TPP derivatives are quite close with values of 3.69, 3.88 and 3.78 Å, respectively, while the L.S. values of the TPP derivatives are quite close [2.53 Å for **1** and 2.83 Å for the OAc derivatives] but lower than the TBrPP derivative [L.S. = 3.321 Å]. An important observation concerns the ~ 0. 1 Å lower Mn···Mn distance of the TBrPP-TCA derivative (which is 4.80 Å) compared to those of the TPP-TCA and TPP-OAc species, with values of 5.57 and 5.87 Å, respectively. This difference is related to the displacement of the manganese atom from the porphyrin mean plane (Mn—P_C). Thus, as mentioned above, the Mn—P_C distances of the TPP-TCA and TBrPP-TCA species are 0.236(1) and 0.147(1) Å, respectively. Therefore, as expected, a large value of Mn—P_C leads to a long Mn…Mn distance. It is noteworthy that π-π dimer formation is also observed in several other iron(III) acetato porphyrin complexes, e.g. for the [Fe^{III}(OEP)(TCA)] derivative, the Fe···Fe, $P_C \ldots P_C$ distances are 5.38 and 4.71 Å, respectively [34].

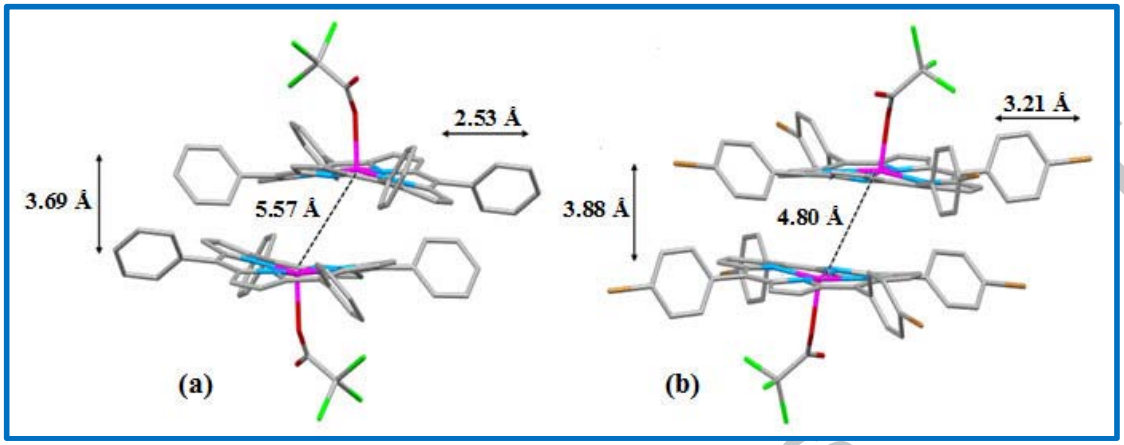

Figure 8. Schematic representations of dimers of **1** (a) and **2** (b).

For **1** and **2**, the two [Mn^{III}(Porph)(TCA)] monomers are linked together by C—H···Cg π intermolecular interactions (Cg are the centroids of the pyrrole and phenyl rings of the porphyrins), leading to dimers (Figures SI-5-6 and Table SI-1).

For complex **1**, (i) the carbon atom C23 of one phenyl ring of a porphyrin of one dimer is weakly linked to the oxygen atom O2 of a TCA ligand of a neighboring dimer (C23—H23···O2), (ii) the carbon atom C24 of the same phenyl ring of a porphyrin for one dimer is weakly bonded to the Cg4 centroid of the same porphyrin of the nearby dimer (C24—H24···Cg4), (iii) the centroid Cg9 of the same phenyl ring for one porphyrin of one dimer is weakly linked to the carbon atom C38 of one phenyl ring of the same nearby dimer (C38—H38···Cg9) and (iv) the carbonyl atom O2 of one TCA ligand from one dimer is linked to the carbon atom C41 of a phenyl ring of a porphyrin of a second dimer (C41—H41···O2) and the same carbon atom C41 is linked to the chlorine atom CL3A of the TCA ligand of the nearest dimer (C41—H41···CL3A).

For complex **2**, the dimer made by two [Mn^{III}(TBrPP)(TCA)] molecules is linked to a nearby dimer by: (i) the centroid Cg10 of a phenyl ring of one porphyrin of this dimer to the carbon atom C22 of a phenyl ring of a porphyrin from the neighbouring dimer (C22—H22···Cg10) and the carbon atom C29 of a phenyl ring of a porphyrin of this dimer to the oxygen atom O1 of the TCA axial ligand of a second dimer (C29—H29···O1). This dimer is also linked to the closest chloroform molecule via (i) the non-conventional H bond C34—H34···Cl4A, where the

C34 atom belongs to a phenyl ring of porphyrin, and the C7—H7···CL4A interaction between the same chlorine atom and the pyrrole carbon atom C7 of a nearby dimer.

4. Conclusion

In the present work, we prepared (trichloroacetato)[5,10,15,20-tetraphenylporphyrinato] manganese(III) [Mn^{III}(TPP)(TCA)] (**1**) and (trichloroacetato)[(5,10,15,20-tetra-(para-bromophenyl)porphyrinato]manganese(III) hemi-chloroform hemi-dichloromethane solvates [Mn^{III}(TBrPP)(TCA)].1/2$CHCl_3$.1/2CH_2Cl_2 (**2**). The UV-visible and ^{1}H NMR spectra show that, in solution, **1** and **2** are high-spin (S = 2) manganese(III) metalloporphyrins and a cyclic voltammetry investigation on **1** and **2** shows similar results to those of the already known Mn(III) porphyrins. The molecular structures of **1** and **2** confirm the high-spin state of **1** and **2** in the solid state and that the TPP derivative (**1**) exhibits higher deformations of the porphyrin macrocycle than the TBrPP species (**2**). The supramolecular structures of **1** and **2** are made by face to face π—π dimers with Mn…Mn distances of 5.57 Å for **1** and 4.80 Å for **2**. These dimers are sustained by weak C—H···Cl, C—H···O and C—H···Cg intermolecular interactions where Cg is the centroid of the pyrrole or phenyl rings.

Acknowledgements

The authors wish to thank Dr Shabir Najmudin for the English revision. The authors gratefully acknowledge financial support from the Ministry of Higher Education and Scientific Research of Tunisia.

Appendix A. Supplementary data

CCDC 1515031 and 1510380 contain the supplementary crystallographic data of complexes **1** and **2**. These data can be obtained free of charge via http://www.ccdc.cam.ac.uk/conts/retrieving.html, or from the Cambridge Crystallographic Data Centre, 12 Union Road, Cambridge CB2 1EZ, UK ; fax: (+44) 1223 336 033; or e-mail: deposit@ccdc.cam.ac.uk. Supplementary data associated with this article can be found, in the online version.

References

[1] D. Mansuy, Coord. Chem. Rev. 125 (1993) 129.

[2] H. Srour, P. Le Maux, S. Chevance, G. Simonneaux, Coord. Chem. Rev. 257 (2013) 3030.

[3] I. Batinic-Haberle, Z. Rajic, A. Tovmasyan, J.S. Reboucas, X.D. Ye, K.W. Leong, M. W. Dewhirst, Z. Vujaskovic, L. Benov, I. Spasojevic, Free Radicals Biol. Med. 51 (2011) 1035.

[4] L. Smith, J.R. Mortimer, D. N, J. Chem. Soc., Perkin Trans. 2 (1986) 1743.

[5] P. N. Balasubramanian, A. Sinha, T.C. Bruice, J. Am. Chem. Soc. 109 (1987) 1456.

[6] W.H. Wong, D. Ostovic, T.C. Bruice, J. Am. Chem. Soc. 109 (1987) 3428.

[7] J.P. Renaud, P. Battioni, J.F. Bartoli, D. Mansuy, J. Chem. Soc., Chem. Commun. (1985) 888.

[8] N. Amiri, P. Le Maux, H. Srour, H. Nasri, G. Simonneaux, Tetrahedron.70 (2014) 8836.

[9] P. Turner, M.J. Gunter, T.W. Hambley, A.H. White, B.W. Skelton, Aust. J. Chem. 51 (1998) 835.

[10] T. Jin, T. Suzuki, T. Imamura, M. Fujimoto, Inorg. Chem. 26 (1987) 1280.

[11] A.D. Adler, F.R. Longo, J.D. Finarelli, J. Goldmacher, J. Assour, L. Korsakoff, J. Org. Chem. 32 (1967) 476.

[12] A.D. Adler, F.R. Longo, F. Kampas, J.J. Kim, Inorg. Nucl. Chem. 32 (1970) 24

[13] SMART, SAINT and SADABS, Bruker AXS Inc., Madison,WI, (2001).

[14] Agilent (2014). CRYSALIS PRO, version 1.171.37.33c. Agilent Technologies, Wroclaw, Poland.

[15] A. Altomare, G. Casacarano, C. Giacovazzo, A. Guagliardi, M.C. Burla, G. Polidori, M. Camalli, J. Appl. Crystallogr. 27 (1994) 435.

[16] M. Nappa, J.S. Valentine, J. Am. Chem. Soc. 100 (1978) 5080.

[17] G.M. Sheldrick, Acta Crystallogr. C71 (2015) 3.

[18] P. McArdle, J. Appl. Crystallogr. 28 (1995) 65.

[19] I. Creanga, A. Palade, A. Lascu, M. Birdeanu, G. Fagadar-Cosma, E. Fagadar-Cosma, Digest J. Nanomater Bios. 10 (2015) 315.

[20] K.S. Suslick, R.A. Watson, S.R. Wilson. Inorg. Chem, 30 (1991) 2311.

[21] K.S. Suslick, R.A. Watson. Inorg. Chem,30 (1991) 912.

[22] P. Turner, M.J. Gunter, B.W. Skelton, A.H. White, T.W. Hambley, J. Chem. Res. 18 (1996) 220.

[23] W. Harhouri, C. Mchiri, S. Najmouddine, C. Bonifácio, H. Nasri, Acta Cryst E.72 (2016) 720.

[24] P. Turner, M.J. Gunter, Inorg. Chem. 33 (1994) 1406.

[25] L.J. Boucher, H.K. Garber. Inorg. Chem. 9 (1970) 2644.

[26] S.L. Kelly, K.M. tric. Inorg. Chem. 21 (1982) 3635.

[27] M. Autret, Z. Ou, A. Antonini, T. Boschi, P. Tagliatesta, K.M. Kadish, J. Chem. Soc., Dalton Trans. (1996) 2793.

[28] W.R. Scheidt, Y. Lee, Struct. Bond. (Berlin), 64 (1987) 1.

[29] J.A. Shelnutt, The Porphyrin Handbook, Vol. 7 pp. 167. (Eds.: K. M. Kadish, K.M. Smith, R. Guilard), Academic Press, San Diego, 7 (2000)

[30] C. Hill, M.M. Williamson, Inorg. Chem. 24 (1985) 2836.

[31] M. Weck, C.W. Jones, Inorg. Chem. 46 (2007) 1865.

[32] Q. Yu, Y. Liu, D. Liua, J. Li, Dalton Trans. 44 (2015) 9382.

[33] J.F. Kirner, C.A. Reed, W.R. Scheidt, J. Am. Chem. Soc. 99 (1977) 2557.

[34] T.J. Neal, B. Cheng, J. Ma, J.A. Shelnutt, C.E. Schulz, W. R. Scheidt, Inorg. Chim. Acta. 291 (1999) 49.

[35] S.A. Mov, J.A. Gonzalez, L.J. Wilson, Acta Cryst. C51 (1995) 1490.

[36] S.A. Yao, C.B. Hansen, J.F. Berry, Polyhedron 58 (2013) 2.

[37] W.R. Scheidt, Y. Lee, Struct. Bond. 64 (2005) 1.

The synthesis of trichloroacetao manganese(III) complexes (**1** and **2**) with *meso*-porphyrins, namely 5,10,15,20-tetraphenylporphyrin (H_2TPP) and the 5,10,15,20-tetra-(*para*-bromophenyl)porphyrin (H_2TBrPP), are described. These two dervatives were characterized by UV/Vis, IR and ^{1}H NMR spectra, which indicate that these Mn(III) complexes are high-spin (S = 2). The cyclic voltammograms of **1** and **2**, and two chloroacetato Mn(III) porphyrins are similar and ressemble those of five-coordinated Mn(III) high-spin porphyrins. Notable, the molecular structures of **1** and **2** exhibit face to face π-π dimer formation with PC···PC distances of 3.69 and 3.88 Å, and Mn···Mn distances of 5.57 and 4.80 Å, respectively.